Supporting Information

Enhancement in the Nonlinear Optical Properties of Silver Nanoprisms through Graphene Oxide Anchoring

*Fadeela Chundekatt Ummer,‡ Hao Yuan,‡ Isabelle Russier-Antoine, Fabien Rondepierre, Pierre-François Brevet, Pierre Mignon, Nandakumar Kalarikkal and Rodolphe Antoine**

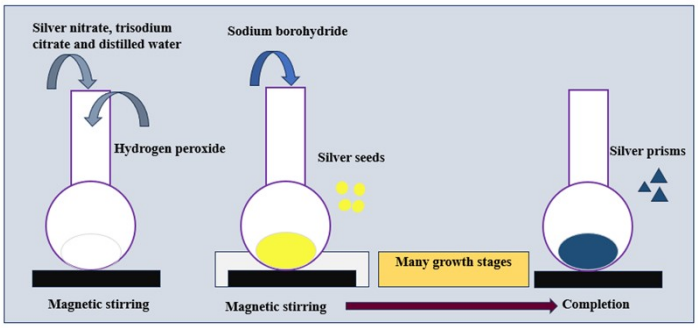

Figure S1: Schematic of synthesis of silver nanoprisms

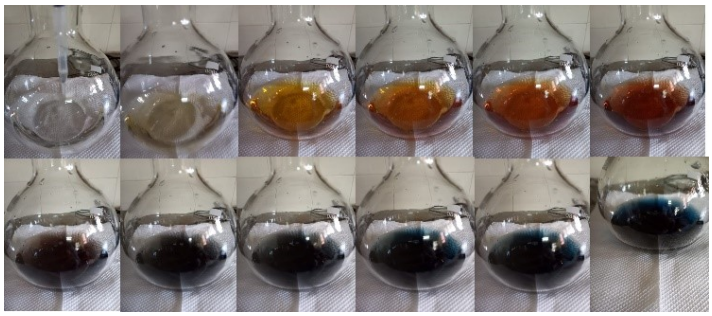

Figure S2: Stages of nanoprisms synthesis

Estimation of concentration of Ag nanoprisms

Concentration of Ag nanoprisms is estimated from the amount of silver, volume of Ag nanoprism and production yield.

Generally, synthesized nanoprisms consist of both expected nanoprisms (AgNPrism) and side production, nanospheres (AgNSphere). AgNPrism content, AgNPrism average edge length, AgNPrism average thickness, and AgNSphere average diameter in the obtained samples were determined from transmission electron microscopy (TEM) images (Figure 2, table and figure below).

Nanoprism content (%)	AgNSphere content (%)	AgNPrism average edge length (nm)	AgNPrism average thickness (nm)	AgNSphere average diameter (nm)
80.88	19.11	30.45	6.72	8.37

AgNPrism average volume $(nm)^3$	AgNSphere Average volume $(nm)^3$
5127.161	306.870

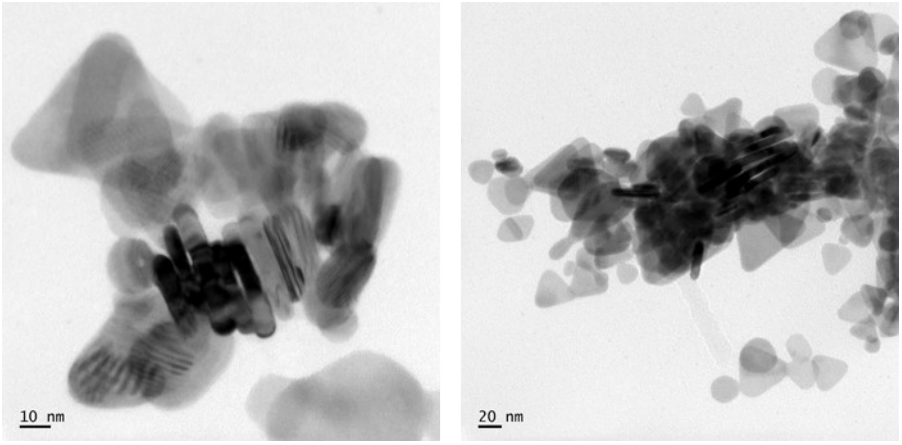

TEM images of silver nanoprisms used for estimating prism thickness.

The number of silver atoms in each nanoparticle was calculated by reported method (J. Anal. At. Spectrom., 2015,30, 245-253, doi: 10.1039/C4JA00225C), considering that the volume ratio of silver atom to AgNSphere/NPrism is 74.1% in the cubic structure, which was proved by (111) plane of silver in high-resolution TEM image (Figure 2(c) and (d)) . The radius of silver atom is 0.144 nm, and therefore its volume is 0.0125 nm^3.

For AgNSpheres with the diameter of *d* nm, as AgNSpheres are spherical in shape, its

volume is $\frac{\pi}{6}d^3$ nm^3. Thus, the number of silver atoms (N) in each AgNSpheres is equal to $\frac{74.1}{100} \times \frac{\pi}{6}d^3 \times \frac{1}{0.0125}$.

$$N(AgNSpheres, 8.37\ nm) = \frac{74.1}{100} \times average\ volume\ (AgNSphere) \times \frac{1}{0.0125} = 18191.25$$

$$N(AgNPrisms, 30.45\ nm) = \frac{74.1}{100} \times average\ volume\ (AgNPrism) \times \frac{1}{0.0125} = 303938.10$$

With the content ratio of AgNPrism: AgNSphere = 80:19, Ag atom ratio for Ag in AgNPrism: Ag in AgNSphere = 80*303938: 19*18191.25=24315048.32: 345629=98.59%: 1.40%.

With the synthesis protocol, the added silver nitrate is totally 100μL*0.1M=$10*10^{-6}$ mol, so Ag atom number input is N(Ag input)=N_A*c=$6.02*10^{23}mol^{-1}*10*10^{-6}$ mol=$6.02*10^{18}$. As the production yield of silver is 37.9%, total Ag atom number in Ag nanoprisms is N (Ag atoms in AgNPrisms) =N(Ag input)* 37.9%*98.59%=$2.25*10^{18}$. Total Ag atom number in AgNSpheres is N (Ag atoms in AgNSpheres) =N(Ag input)* 37.9%*1.40%=$0.032*10^{18}$.

$$Concentration\ of\ AgNSphere = \frac{N(Ag\ atoms\ in\ AgNSpheres)}{N(AgNSpheres, 8.37\ nm) * V * N_A} = \frac{0.032 * 10^{18}}{18191.25 * 0.1\ L * 6.02 * 10^{23} mol^{-1}} = 2.92 * 10^{-11}\ M$$

$$Concentration\ of\ AgNprism = \frac{N(Ag\ atoms\ in\ AgNPrisms)}{N(AgNPrisms, 30.45\ nm) * V * N_A} = \frac{2.25 * 10^{18}}{303938 * 0.1\ L * 6.02 * 10^{23} mol^{-1}} = 1.23 * 10^{-10} M$$

The sum concentration of AgNSpheres and AgNPrisms, $1.522 * 10^{-10} M$, was used for further calculation and characterization, as the concentration of silver nanoprisms. Ag nanospheres and Ag nanoprisms could be considered as a whole system, which is called 'silver nanoprisms' in this work. This mother solution of silver nanoprisms was diluted for futher coupling with graphene oxide, and the concentration could be calculated by dilution times.

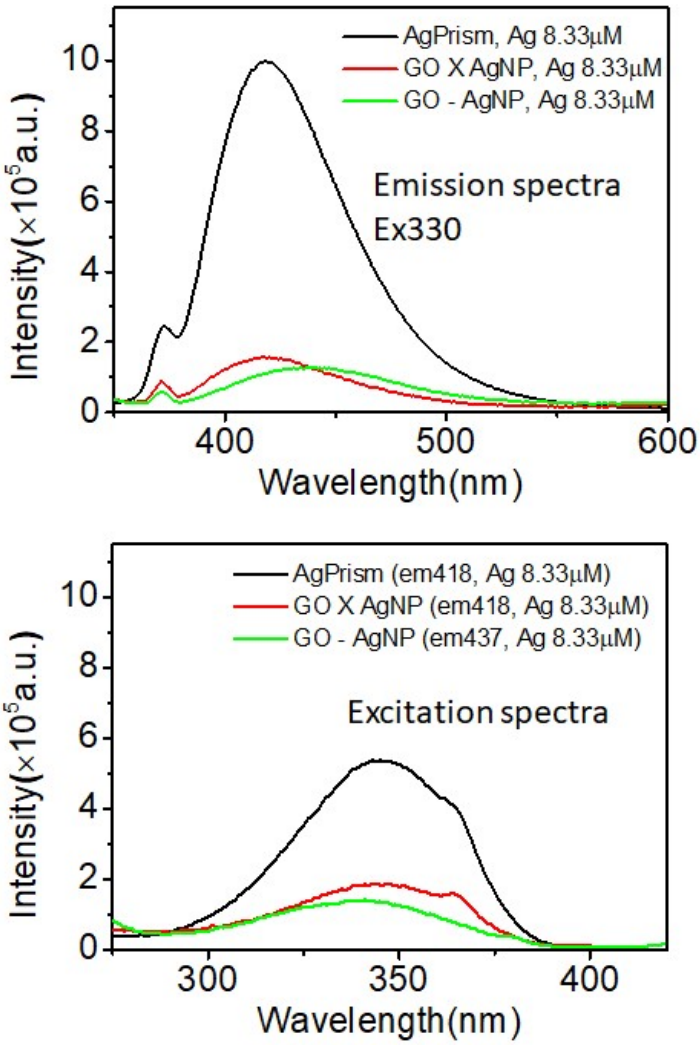

Figure S3: Photoluminescence emission and excitation spectra of silver nanoprisms and silver nanocomposites (GO-Ag and GO-X-Ag) diluted in water. Concentration Ag nanoprisms: 2.54 pM.

Table S1: The fitted parameters of Raman spectrum.

Sample	D band (cm^{-1})	FWHM	G band (cm^{-1})	FWHM
GO	1350	176.775	1593	93.108
GO-Ag	1346	176.418	1590	93.688
GO-X	1348	182.890	1590	97.605
GO-X-Ag	1346	182.904	1593	97.594

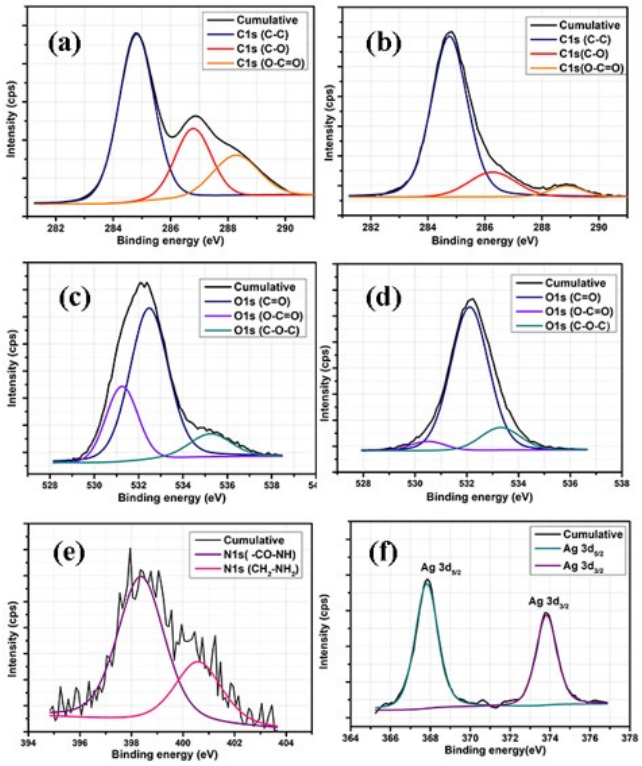

Figure S4: Deconvoluted XPS spectra (a) C1s of GO-Ag (b) C1s of GO-X-Ag (c) O1s of GO-Ag (d) O1s of GO-X-Ag (e) N1s of GO-X-Ag and (f) Ag of GO-Ag.

Additional characterization of silver – GO nanocomposites

To understand the chemical states of the hybrids, detailed FTIR spectral investigations of the hybrids and their constituents is carried out. The assignments of various FTIR peaks are as follows. Figure S5(a) shows the FTIR spectra of silver nanoprisms (Ag), graphene oxide (GO), and graphene-oxide silver composite (GO-Ag) prepared by the physical mixing of both components. The FTIR spectra of triangular silver nanoprisms show typical peaks at 3328 cm^{-1}, 2958 cm^{-1}, 2924 cm^{-1}, 2856 cm^{-1}, 1579 cm^{-1},1445 cm^{-1},1369 cm^{-1},1249 cm^{-1},1078 cm^{-1}, and 1018 cm^{-1}. The wide band at 3328 cm^{-1} is due to the O-H stretching vibrations. The peaks at 2958 cm-1,2924 cm^{-1}, and 2856 cm^{-1} are due to the stretching vibrations of Csp3-H bonds of the citrate molecule. The peak at 1579 cm^{-1} and 1369 cm^{-1} is associated with the asymmetric and symmetric C=O stretching of the carboxylate functional groups of citrates coordinated with silver ions. The peak at 1445 cm^{-1} is likely due to the C=O symmetric stretching of carboxylate groups of free citrate groups present in the sample. A less intense peak at 1249 cm^{-1} is due to the C-O stretching of the carboxylic acid group also present in the FTIR spectrum.[1-4]

The FTIR spectrum of graphene oxide shows peaks at 3236 cm^{-1}, 2975 cm^{-1}, 1702 cm^{-1}, 1578 cm^{-1}, 1411 cm^{-1}, 1241 cm^{-1}, 1145 cm^{-1}, and 1022 cm^{-1}. The peak at 3236 cm^{-1} is due to the stretching vibrations of -OH (hydroxyl) groups present in the graphene oxide basal planes, and the peak at 2975 cm^{-1} is due to asymmetric Csp3-H stretching. The peak at 1702 cm^{-1} is due to the C=O stretching carbonyl groups, and the peak at 1578 cm^{-1} is due to aromatic C=C skeletal vibrations of the graphitic planes. The peak at 1411 cm^{-1} is due to the O-H deformations, and the peak at 1022 cm^{-1} is due to C-O-C stretching vibrations of the epoxy group present in graphene oxide sheets.[5-9]

The FTIR spectra of the GO-Ag hybrid show characteristic peaks at 3236 cm^{-1}, 2975 cm^{-1},2881 cm^{-1}, 1574 cm^{-1}, 1469 cm^{-1}, 1255 cm^{-1}, 1141 cm^{-1}, and 1073 cm^{-1}. The hybrid also shows characteristic peaks of citrate-capped silver prisms such as 1469 cm^{-1}, 1371 cm^{-1}, and 1073 cm^{-1}, along with the peaks of graphene oxide. The intensity of the -OH stretching peak (3236 cm^{-1}) is reduced considerably in the hybrid due to the possible chemical reduction of graphene oxide in the presence of citrate groups. Interestingly, the peak characteristic of free citric acid C=O stretching at 1445 cm^{-1} is absent in the FTIR spectrum of the GO-Ag hybrid. This observation strengthens the argument for the chemical reduction of GO in the presence of free citrate molecules.[10, 11]

Figure S5(b) shows the FTIR peaks of covalently functionalized graphene oxide (GO-X) and its hybrid with silver nano prism (GO-X-Ag). The FTIR peak of GO-X shows characteristic peaks at 3355 cm^{-1}, 3222 cm^{-1},2981 cm^{-1},2885 cm^{-1},1636 cm^{-1},1602 cm^{-1},1547 cm^{-1}, 1501 cm^{-1},1249 cm^{-1},1156 cm^{-1},1026 cm^{-1} and 940 cm^{-1}. The 'W' shaped curve with peaks at 3355 cm^{-1} and 3222 cm^{-1} corresponds to the asymmetric and symmetric stretching N-H vibrations (see Figure S6). The peaks at 2981 and 2885 cm^{-1} are due to Csp3-H vibrations. The peak at 1636 cm^{-1} is owing to the C=O stretching of the amide formed. The peak at 1602 cm^{-1} is due to the aromatic C=C stretching of the functionalized graphene oxide skeleton. The peak at 1547 cm^{-1} is due to the characteristic N-H deformation of secondary amide. The peak at 1501 cm^{-1} is due to the C-N stretching vibrations of amides. The peak corresponding to O-H deformation (1411 cm^{-1}) absent in the spectrum indicates the formation of the amide group upon reaction of GO with ethylene diamine. The peaks at 1156 cm^{-1} are due to the stretching vibration of amine groups. The peak at 940 cm^{-1} is typical of the C-H deformation, indicating the successful functionalization of graphene oxide with amine. In the FTIR spectrum of GO-X-Ag, the redshifted C=O stretching peak at 1698 cm^{-1}(of amide) and a redshifted broad peak at 1577 cm^{-1} (N-H deformation of secondary amide) indicates that the further amide formation, when integrated with citrate capped silver nano prisms. The broad peak may be due to the overlapping of several FTIR peaks characteristic of amine-functionalized graphene oxide and citrate-capped silver nano prisms. This observation also supports the broad peak around 3364 cm^{-1} instead of the 'W' shaped curve as in GO-X. In addition to this, we can see that all the peaks characteristic of graphene oxide (GO-X) and silver nano prisms are redshifted in the hybrid.[5, 12-14]

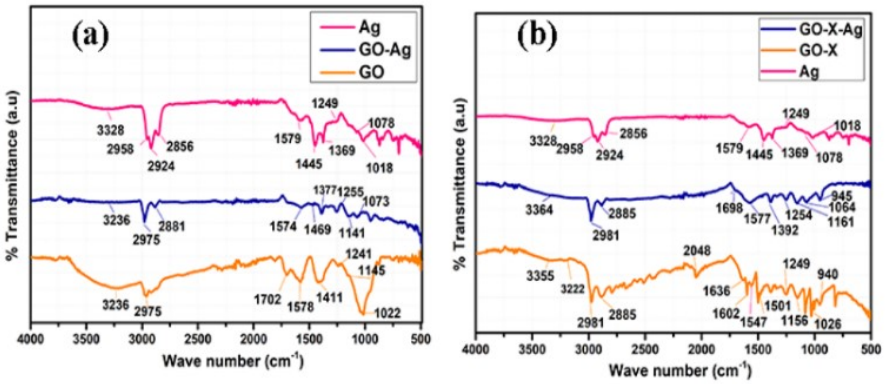

Figure S5: (a) FTIR spectra of silver nano prism , GO, GO-Ag (b) GO-X and GO-X-Ag

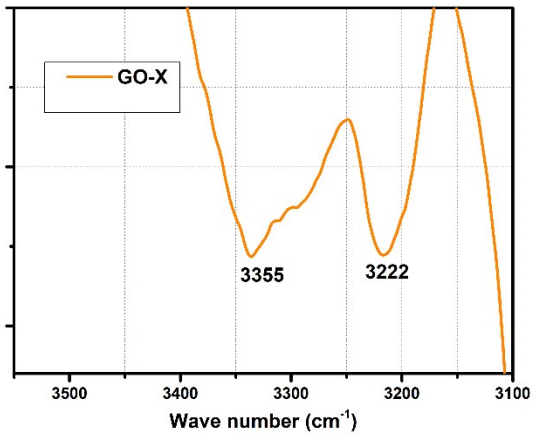

Figure S6: asymmetric and symmetric stretching N-H vibrations of GO-X

Figure S7(a) and S7(b) shows the confocal Raman images of GO-Ag and GO-X-Ag. This image shows that the silver nano prisms are more uniformly decorated over the graphene oxide rather than the covalently functionalized graphene oxide. During the covalent functionalization of the graphene oxide, it is visible that the dispersion is slightly coagulated, and stability of its dispersion in water is slightly affected. The slight coagulation of graphene oxide due to amino functionalization may be the reason for the non-uniform distribution of silver nano prisms over the covalently functionalized graphene oxide.

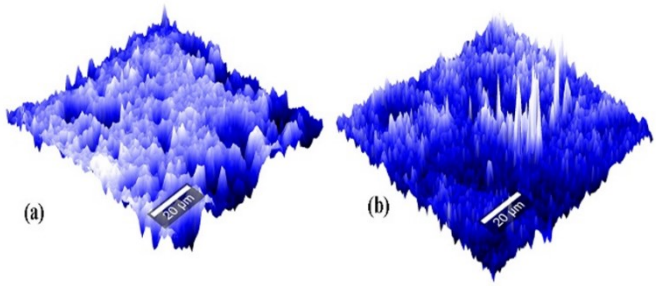

Figure S7: (a) Confocal Raman mapping GO-Ag (b) and GO-X-Ag showing the distribution of silver in graphene oxide matrix (White region shows silver and blue region shows graphene oxide).

Figure S8 shows the XRD pattern of graphene oxide (GO) and covalently functionalized graphene oxide with ethylene diamine (GO-X). The graphene oxide shows the characteristic diffraction peak at 2θ value 11.21° with a d spacing value of 0.788 nm corresponding to the (001) plane of graphene oxide. At the same time, the diffraction peak of covalently functionalized graphene oxide is at 2θ value 9.6° with a d spacing of 0.919 nm. The peak shifts to a lower 2θ value with increased d-spacing, indicating that -NH2 groups are covalently attached to the graphene oxide basal plane. The decreased FWHM indicates the more ordered structure of GO-X compared to GO. These findings are consistent with Raman spectra.[15, 16]

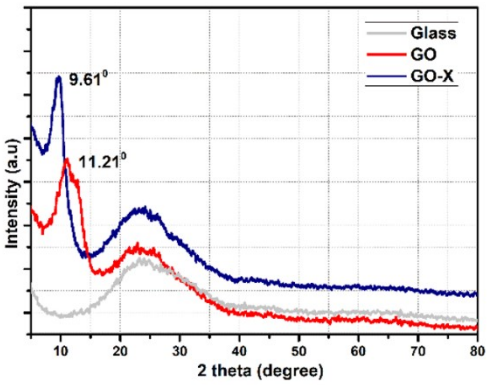

Figure S8: XRD pattern of GO and GO-X-Ag

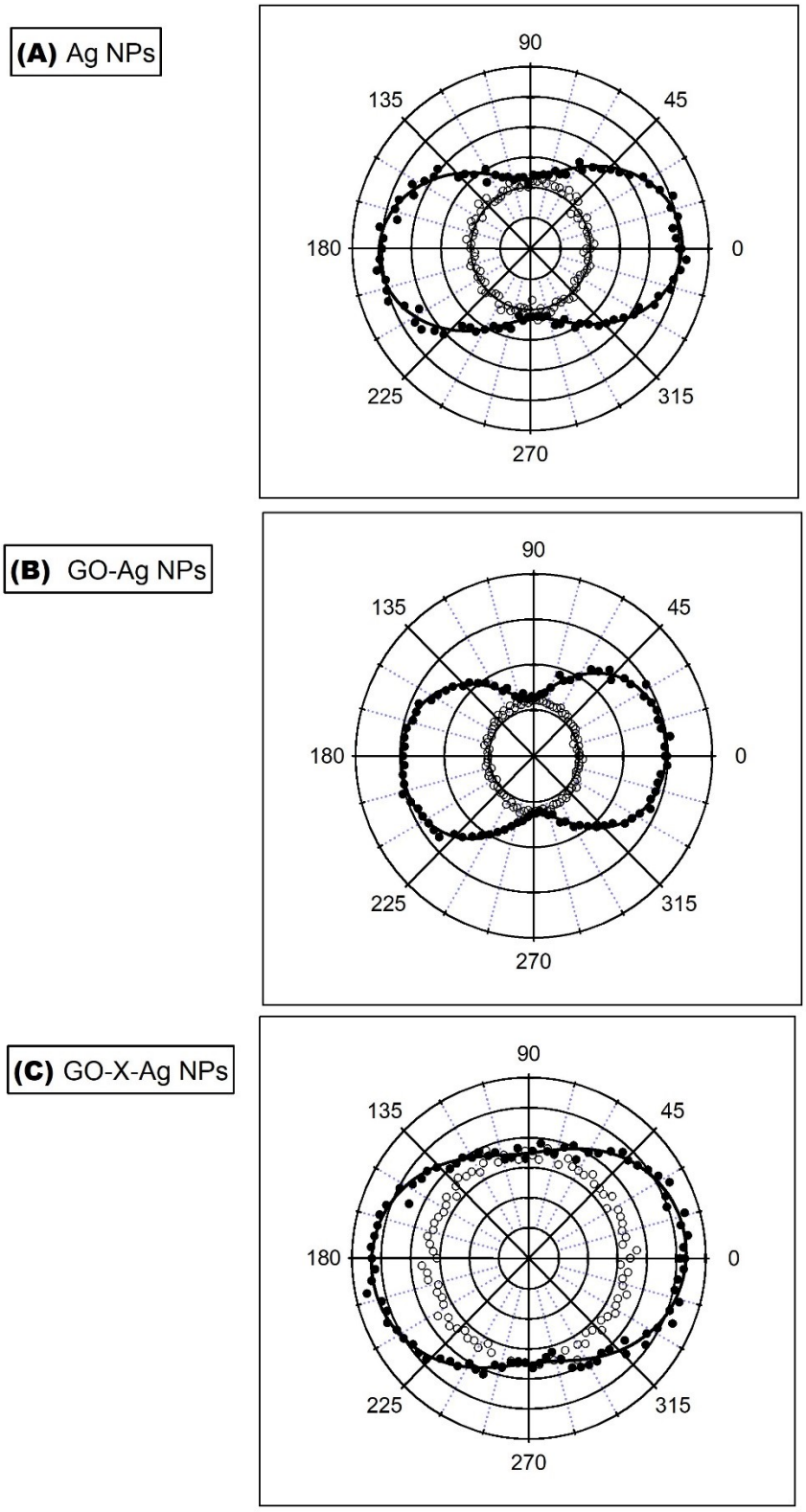

Figure S9: Polar plots of (A) Ag, (B) GO-Ag and (C) GO-X-Ag NPs

Table S2: Depolarization and retardation parameters obtained for the three samples, Ag NPs, GO-Ag and GO-X-Ag.

samples	retardation parameter	depolarization ratio
silver nanoprisms	-0.04 ± 0.01	0.45 ± 0.02
GO-Ag nanocomposites	0.19 ± 0.01	0.43 ± 0.02
GO-X-Ag nanocomposites	0.04 ± 0.01	0.65 ± 0.03

Polarization plots for the three samples were adjusted with the following equation :

$$I_{HRS}^{\Gamma} = a^{\Gamma}cos^4\gamma + b^{\Gamma}cos^2\gamma sin^2\gamma + c^{\Gamma}sin^4\gamma \qquad \text{(S1)}$$

where γ stands for the fundamental beam angle of polarization and Γ for the harmonic light angle of polarization with $\gamma,\Gamma = 0$ for the polarization perpendicular to the scattering plane. One can then define the depolarization parameter as c^V/a^V and the retardation parameter as $(b^V - a^V - c^V)/b^V$, see ref. [S1]. The depolarization parameter assesses the symmetry of the nonlinear optical source to the second harmonic light, a value of 2/3 indicating a purely octupolar symmetry. The retardation parameter provides the extent of deviation from a purely incoherent response. Table S2 gives those two parameters characterizing the polarization plots for the three Ag NPs, GO-Ag and GO-X-Ag samples.

[S1] Duboisset J., Brevet P.F., Second-Harmonic Scattering-Defined Topological Classes for Nano- Objects, J. Phys. Chem. C, 2019, 123, 25303-25308.

Computational Details

Models construction: according to XPS measurements and related quantitative analyses, element's content ratios have been evaluated allowing to quantify the amount of hydroxyl and peroxide groups on GO.

Quantitative XPS results of GO-Ag and GO-X-Ag

Sample Name	C	O	Ag	N
GO-Ag	54.2	45.8	0.1	-
GO-X-Ag	59.1	40.0	<.01	0.9

Quantitative analysis of C1s of GO-Ag and GO-X-Ag from the area under the curve of each peak

Sample Name	% of C-C (284.82 eV)	% of C-O (286.79eV)	% of O-C=O (288.31 eV)
GO-Ag	51.93	24.56	23.49
GO-X-Ag	78.74	16.10	5.14

According to these data and the initial graphene model (10x10x1 graphene supercell) counting to 200 C atoms and the number of atoms of the citrate molecule.

Since we will not model the edges of graphene we will reproduce only the proportion of oxygen atoms present in hydroxyl and epoxy groups as compared to the total number of C atoms. In addition, it can be predicted that the proportion of COOH in the two systems is the same. The only things that changes is that in GO-X-Ag the CCOOH are changed with the chemisorbed molecules. As such we will only consider a system with a regular number of oxygen (belonging to hydroxyl and epoxy groups) as compared to C atoms equilibrated from a proportion of CO and COOH groups …

For full GO => NC = 200

- Nog = Nc / %c – Nc – Nom = 200/0.542-200-7 = 162.00
- among 162 Og, it counts 1O per CO and 2O per COOH,
    - proportion of O in CO groups among all O belonging to CO et COOH :
        - %co / (%co+%cooh) = 24.56/(24.56+23.49 *2) = 0.3433
        - So : 162*0.3433 = 55.61 = 56 O (belonging to hydroxyl or epoxy groups)

As such the 10 x 10 x 1 graphene supercell has been randomly grafted with 40 OH and

15 epoxy on each side of the sheet and respecting a C atom between two O/OH grafting. 6 models have been built and optimized, those exhibiting reactivity between OH and epoxide groups forming OHO bridges or ejecting a water molecule where excluded and the structure with the lower energy was retained. The geometry relaxations consisted in optimizing consecutively supercell parameters and ionic positions independently allowing well describe ionic relaxation at fix cutoff energy (since cutoff energy depend on the supercell volume. The final GO parameters for the electrostatic model are a=24.63Å, b=24.61Å, c=14.7Å, α=90°, β=90°, γ=60°.

Figure S10. Geometry of the electrostatic GO model

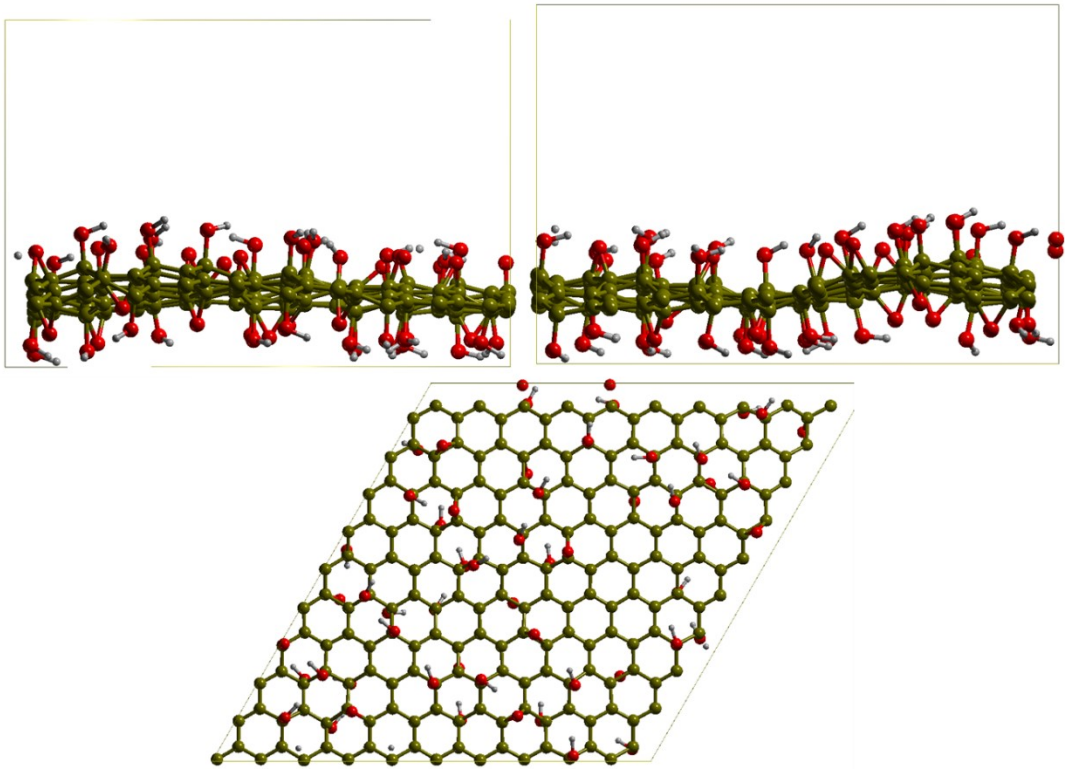

For the covalently bond model, the GO has been constructed by including a hole defect in the supercell from the removal of 15 C atoms, and the randomly grafting of 25 hydroxyl and 8 epoxy groups. On one edge C atom a COOH group has been grafted, in order to further include the NH-$[CH_2]_2$-NH-CO-citrate moiety (see figure S6). Again 6 models were randomly built and the one showing no reactivity during the relaxation procedure with the lowest energy was retained. The final GO parameters for the covalently bond model are a=24.60Å, b=24.58Å, c=14.64Å, α=90°, β=90°, γ=60°.

Figure S11. Geometry of the covalently bond GO model.

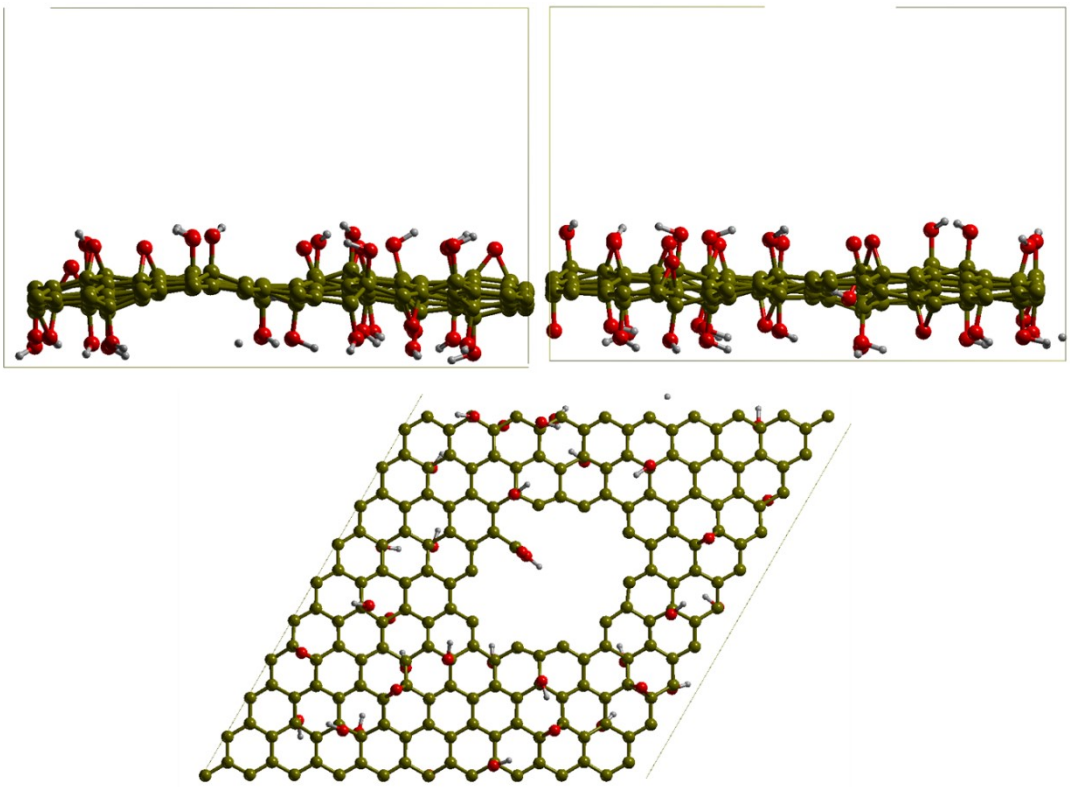

GO-Ag_1, GO-Ag_2 and GO-X-Ag complexes.

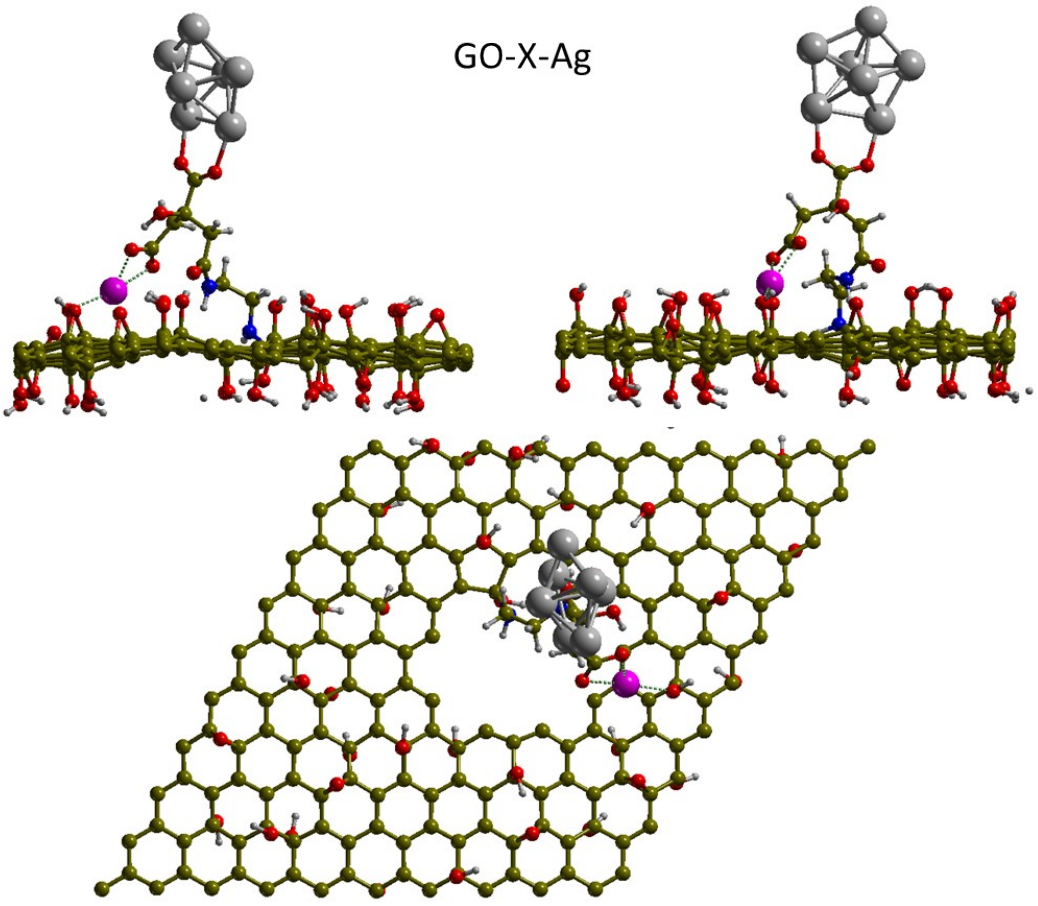

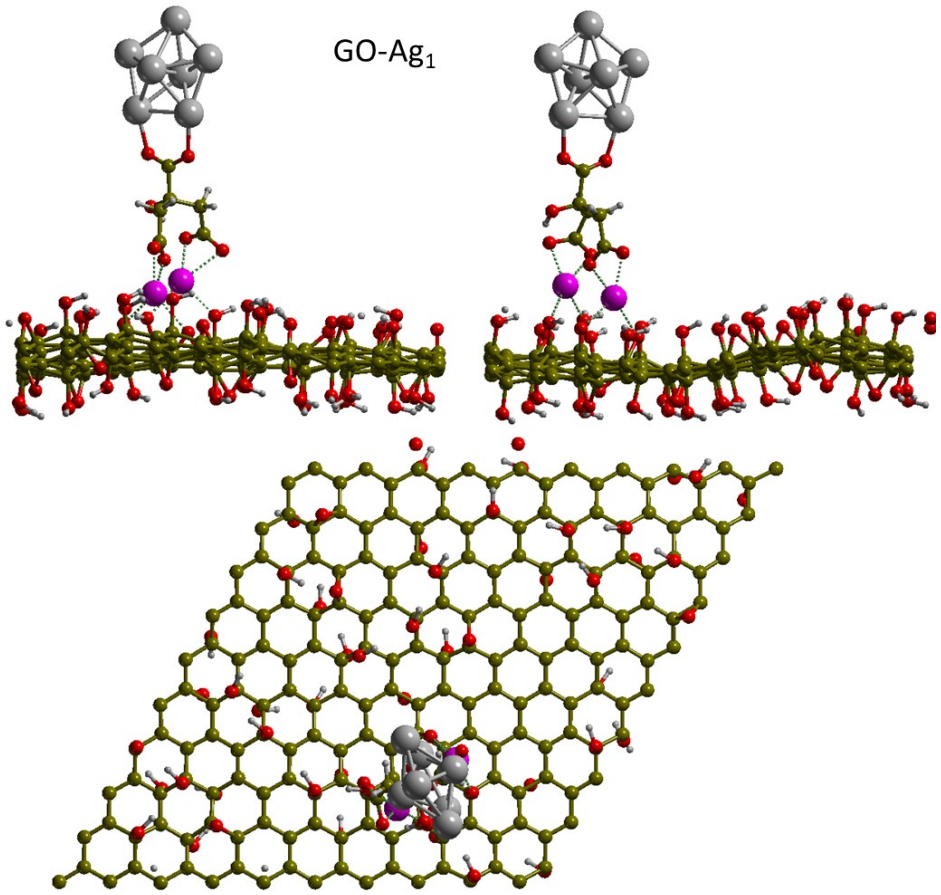
GO-Ag1

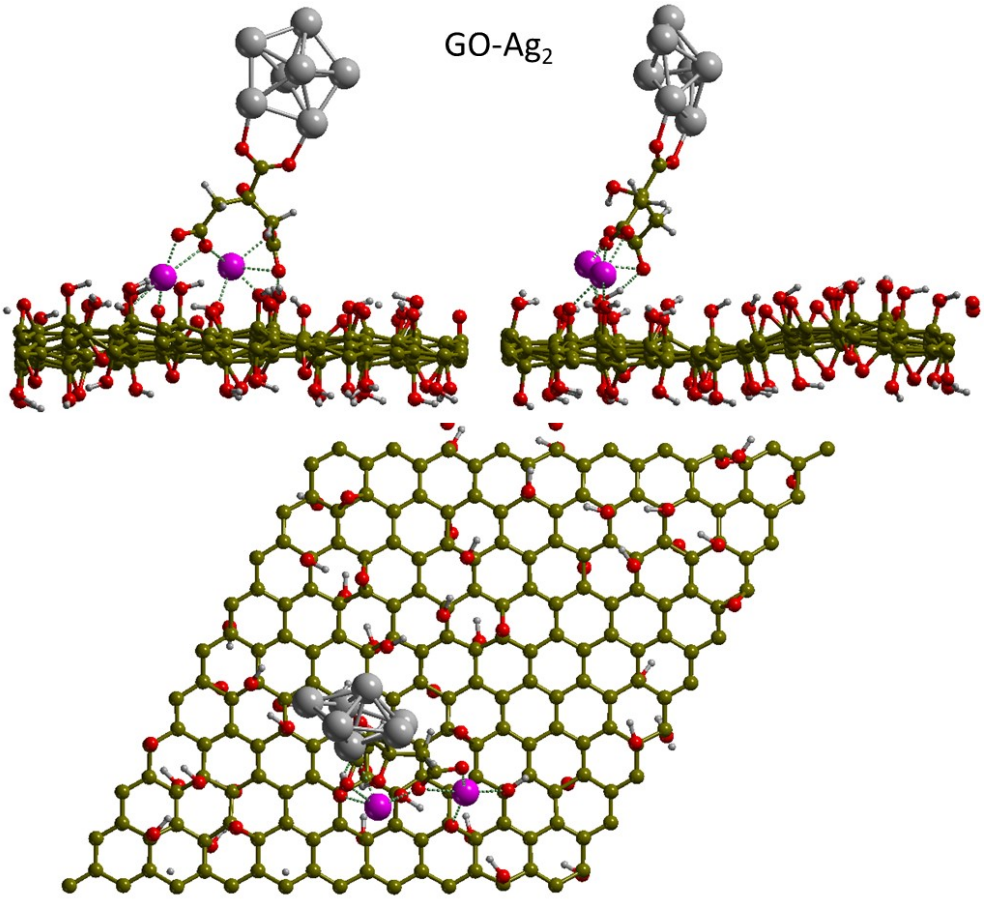
GO-Ag2

References:

1. M. S. Frost, M. J. Dempsey and D. E. Whitehead, *Colloids and Surfaces A: Physicochemical and Engineering Aspects*, 2017, **518**, 15-24.
2. T. H. N. Nguyen, T. D. Nguyen, M. T. Cao and V. V. Pham, *Colloids and Surfaces A: Physicochemical and Engineering Aspects*, 2020, **594**, 124659.
3. K. Ranoszek-Soliwoda, E. Tomaszewska, E. Socha, P. Krzyczmonik, A. Ignaczak, P. Orlowski, M. Krzyzowska, G. Celichowski and J. Grobelny, *Journal of Nanoparticle Research*, 2017, **19**, 273.
4. P. Wulandari, T. Nagahiro, N. Fukada, Y. Kimura, M. Niwano and K. Tamada, *Journal of Colloid and Interface Science*, 2015, **438**, 244-248.
5. L. Mei, C. Lin, F. Cao, D. Yang, X. Jia, S. Hu, X. Miao and P. Wu, *ACS Applied Nano Materials*, 2019, **2**, 2902-2908.
6. T. Naseem, A. Zain ul, M. Waseem, M. Hafeez, S. U. Din, S. Haq and R. Mahfoz ur, *Journal of Inorganic and Organometallic Polymers and Materials*, 2020, **30**, 3907-3919.
7. G. Surekha, K. V. Krishnaiah, N. Ravi and R. Padma Suvarna, *Journal of Physics: Conference Series*, 2020, **1495**, 012012.
8. D. S. Sutar, P. K. Narayanam, G. Singh, V. D. Botcha, S. S. Talwar, R. S. Srinivasa and S. S. Major, *Thin Solid Films*, 2012, **520**, 5991-5996.
9. X. Liu, J. Yang, W. Zhao, Y. Wang, Z. Li and Z. Lin, *Small*, 2016, **12**, 4077-4085.
10. V. Agarwal and P. B. Zetterlund, *Chemical Engineering Journal*, 2021, **405**, 127018.
11. W. Wan, Z. Zhao, H. Hu, Y. Gogotsi and J. Qiu, *Materials Research Bulletin*, 2013, **48**, 4797-4803.
12. S. M. Mousavi, S. A. Hashemi, M. Arjmand, A. M. Amani, F. Sharif and S. Jahandideh, *ChemistrySelect*, 2018, **3**, 7200-7207.
13. B. Ramezanzadeh, S. Niroumandrad, A. Ahmadi, M. Mahdavian and M. H. M. Moghadam, *Corrosion Science*, 2016, **103**, 283-304.
14. M. G. Song, J. Choi, H. E. Jeong, K. Song, S. Jeon, J. Cha, S.-H. Baeck, S. E. Shim and Y. Qian, *Applied Surface Science*, 2020, **529**, 147189.
15. A. Navaee and A. Salimi, *RSC Advances*, 2015, **5**, 59874-59880.
16. S. Rani, M. Kumar, R. Kumar, D. Kumar, S. Sharma and G. Singh, *Materials Research Bulletin*, 2014, **60**, 143-149.